

# Electronic and magnetic properties of VOCl/FeOCl antiferromagnetic heterobilayers

F. Mahrouche,<sup>1,2</sup> K. Rezouali,<sup>1</sup> Z. C. Wang,<sup>3</sup> J. Fernández-Rossier,<sup>3</sup> and A. Molina-Sánchez<sup>4</sup>

<sup>1</sup>*Laboratoire de Physique Théorique, Faculté des Sciences Exactes, Université de Bejaia, 06000 Bejaia, Algérie*

<sup>2</sup>*Departamento de Física Aplicada, Universidad de Alicante, 03690 San Vicente del Raspeig, Spain*

<sup>3</sup>*QuantaLab, International Iberian Nanotechnology Laboratory (INL), 4715-330 Braga, Portugal*

<sup>4</sup>*Institute of Materials Science (ICMUV), University of Valencia, Catedrático Beltrán 2, E-46980, Valencia, Spain*

We study the electronic properties of the heterobilayer of vanadium and iron oxychlorides, VOCl and FeOCl, two layered air stable van der Waals insulating oxides with different types of antiferromagnetic order in bulk: VOCl monolayers are ferromagnetic (FM) whereas the FeOCl monolayers are antiferromagnetic (AF). We use density functional theory (DFT) calculations, with Hubbard correction that is found to be needed to describe correctly the insulating nature of these compounds. We compute the magnetic anisotropy and propose a spin model Hamiltonian. Our calculations show that interlayer coupling is weak and ferromagnetic so that magnetic order of the monolayers is preserved in the heterobilayers providing thereby a van der Waals heterostructure that combines two monolayers with different magnetic order. Interlayer exchange should lead both to exchange bias and to the emergence of hybrid collective modes that combine FM and AF magnons. The energy band of the heterobilayer show a type II band alignment, and feature spin-splitting of the states of the AF layer due to the breaking of the inversion symmetry.

## I. INTRODUCTION

The observation of magnetic order in stand-alone monolayers<sup>1-3</sup> derived from van der Waals layered magnetic compounds has started a new research area in 2D materials with potential for applications in spintronics.<sup>4</sup> Magnetic 2D crystals have also non-trivial physical properties such as topological magnons,<sup>5,6</sup> skyrmions,<sup>7</sup> or quantized anomalous Hall effect.<sup>8,9</sup> Moreover, the study of Van der Waals heterostructures combining magnetic and non magnetic materials,<sup>10</sup> as well as different types of magnetic materials, creates a huge space of opportunities to create artificial structures with novel properties.<sup>11</sup> This includes functional devices, such as spin filter tunnel junctions,<sup>12</sup> as well as heterostructures where magnetic proximity effect promotes spin splitting in otherwise non-magnetic materials<sup>10</sup> as well as the emergence of topological superconductivity.<sup>11</sup>

Here we choose to study heterobilayers made of two magnetic oxides like vanadium and iron oxychloride (VOCl<sup>13-16</sup> and FeOCl<sup>17,18</sup>). Bulk FeOCl undergoes a paramagnetic to antiferromagnetic transition at  $92 \pm 3$  K, according to Mossbauer spectra<sup>19</sup> with antiferromagnetic order in the monolayers. In contrast, neutron scattering experiments<sup>14,20</sup> shows that bulk VOCl is formed by antiferromagnetically coupled monolayers with ferromagnetic order, very much like CrCl<sub>3</sub>.<sup>21</sup> The Neel temperature of VOCl was reported to be 80 K.<sup>14,20</sup> Recently, the ferromagnetic phase of VOCl was reported at 150 K.<sup>22</sup> Importantly, both FeOCl<sup>23</sup> and VOCl<sup>24</sup> are insulating.

Moreover, FeOCl has a unique catalytic structure<sup>25</sup> and VOCl has potential as electrode material in rechargeable lithium-ion batteries.<sup>26,27</sup> Theoretical studies have demonstrated that the bulk VOCl system has a strong magnetoelastic coupling that might be used for development of magnetoelastic sensors and actuators.<sup>14</sup>

Apart of the current applications, our initial motiva-

tion to look into VOCl and FeOCl comes from the fact that degradation of samples exposed to air has been a practical obstacle in the experimental research on most magnetic 2D crystals. In principle, we expect that magnetic oxides are not affected by this problem, showing good air stability in recent studies.<sup>22</sup> In addition, most of the work so far has focused on ferromagnetic compounds, with the notable exception of MPS<sub>3</sub> (M=Mn,Fe, Ni).<sup>28</sup>

Another reason to study these compounds comes from their lattice structure. The magnetic atoms in FeOCl and VOCl form a square lattice, different from the honeycomb lattices of the chromium trihalides<sup>29</sup> or FePS<sub>3</sub>.<sup>1,2</sup> This may bring new possibilities in the study of moire magnets<sup>30</sup> or in the study of proximity effects.<sup>31</sup>

In this work we address the electronic and magnetic properties of van der Waals heterobilayers made of monolayers of FeOCl and VOCl. We explore emergent properties in the composite system that are missing in the constituent layers. We find that ferromagnetic (antiferromagnetic) order is preserved in the VOCl (FeOCl) monolayers, both on their own and forming part of a heterobilayer. We also report a type-II band alignment, useful for hosting long-lifetime excitons,<sup>32</sup> and a spin splitting of the otherwise spin degenerate bands of FeOCl in the range of 2 meV.

The manuscript is organized as follows. In Section II we briefly describe the application of density functional theory together with the Hubbard correction to obtain the main properties of monolayers and FeOCl/VOCl bilayers. In Section III we present our results for the monolayers and compare with the existing literature. In section IV we present the results for the heterobilayer. In Section V we present our conclusions.

## II. METHODS

We apply density functional theory (DFT),<sup>33</sup> within the generalized gradient approximation (GGA), Perdew-Burke-Ernzerhof (PBE) parameterization,<sup>34</sup> and the projector augmented-wave (PAW) method, including spin-orbit coupling, as implemented in the Vienna ab initio simulation package (VASP).<sup>35,36</sup> The electronic correlation of the  $d$  orbitals of Fe and V is computed with the Hubbard correction with values of 5.3 and 2.0 eV for  $d$  orbitals of Fe and V, respectively.<sup>37,38</sup> In heterobilayers, the van der Waals interaction is accounted with the DFT-D3 method.<sup>39</sup>

The lattice constants and internal coordinates are optimized until the residual forces on each atom are less than 0.01 eV/Å. We have optimized using GGA+U. For all systems, a basis-set cutoff energy of 520 eV is used, and the sampling of the Brillouin zone (BZ) is a  $10 \times 8 \times 1$   $\mathbf{k}$ -grid. A vacuum layer of 20 Å is set in the out-of-plane direction to avoid unphysical interactions between periodic replicas.

The crystal structure of monolayer FeOCl and VOCl, together with the FeOCl/VOCl heterobilayer is shown in Fig. 1. The space group for monolayers is  $D_{2h}$  and the point symmetry is  $C_{2v}$ . In the case of the bilayer the point symmetry is also  $C_{2v}$ . The monolayer in-plane lattice parameters are  $a = 3.281$  Å,  $b = 3.836$  Å for FeOCl and  $a = 3.341$  Å,  $b = 3.843$  Å for VOCl. In the case of the heterobilayer, the in-plane parameters are  $a = 3.311$  Å,  $b = 3.840$  Å, while the interlayer separation is  $d = 3.69$  Å, as indicated in Fig. 1. The results of the structural optimization are in good agreement with previous works.<sup>19,40,41</sup>

## III. ELECTRONIC AND MAGNETIC PROPERTIES OF MONOLAYERS

### A. Ab initio calculations

Based on a simple analysis of the chemical valence of the atoms in both compounds, we expect that both Fe and V are in the +3 the oxidation state assuming that O and Cl have valence -2 and -1, respectively. In the case of FeOCl, the external shell of  $\text{Fe}^{3+}$  is  $3d^5$  and in the ionic limit relevant for an insulator, first Hund's rule predicts a spin  $S_{\text{Fe}} = 5/2$ , and thereby a magnetic moment  $M_{\text{Fe}} = 5\mu_B$ . Our calculations give  $M_{\text{Fe}} = 4.8\mu_B$ , not far from the naive ionic picture. We have also found some residual magnetization of O and Cl atoms. Analogously, for VOCl the external shell of  $\text{V}^{3+}$  is  $3d^2$ , and we expect an atomic spin  $S_{\text{V}} = 1$ , and a magnetic moment  $M_{\text{V}} = 2\mu_B$ . In our calculations we found  $M_{\text{V}} = 1.7\mu_B$ , in line with the results for FeOCl.

From the ionic picture, V and Fe are not closed shell. Therefore, an important question is whether the  $3d$  electrons form itinerant bands or, on the contrary, a bandgap opens due to either crystal field splitting of the  $3d$  levels or to correlation effects. From our DFT calculations we conclude that a bandgap only opens in FeOCl and VOCl monolayers when the Hubbard  $U$  is included in the calculations, both when considering ferromagnetic (FM) and antiferromagnetic (AF) order on the layers. As we discuss below, we find that FeOCl monolayers are AF whereas VOCl monolayers are FM.

Regarding the electronic bandgap, in both semiconductors the bandgap is indirect. Nevertheless, in VOCl the conduction band (CB) minima is very close to the high symmetry point  $S$ , in which yields the valence band (VB) maxima. Considering the relative flat bands at VB and CB edges, the absorption/emission should be still comparable to that of direct 2D materials.

Figure 2 shows the band structures of FeOCl and VOCl monolayers computed with PBE+ $U$  in the AF and FM phase, respectively, together with the projected DOS. In the case of FeOCl the hybridization of Fe  $d$  orbitals with the Cl and O atomic orbitals is very strong, as shown in the projected DOS of the valence band. Note that the conduction band is purely composed by iron. Moreover, the bands of FeOCl are doubly degenerate as expected on an antiferromagnet with an inversion center. In the case of VOCl the situation is pretty different, for two reasons: first, hybridization with O and Cl in both valence and conduction bands is very weak. Second, both valence and conduction bands are spin polarized, with spin projection along the majority spin direction. We note that the top of the valence band of VOCl has a two-fold orbital degeneracy along the  $SY$  and  $SX$  directions.

In order to determine both the type of magnetic order and the magnetic anisotropy, we have carried out PBE+ $U$  calculations considering both FM and AF configurations with spin pointing along four directions [100], [010], [001], and [110]. A summary of the ground state

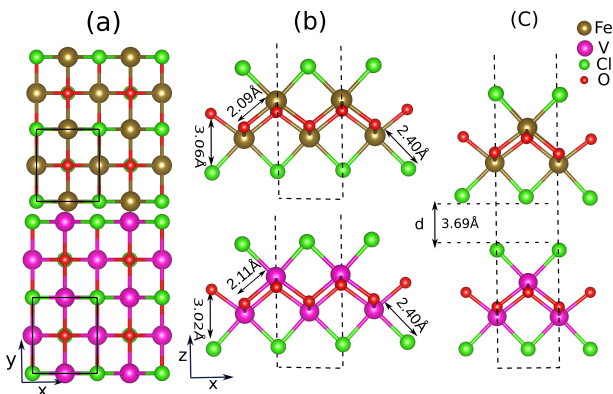


FIG. 1. (Color online) Top (a) and side (b) view of structure of FeOCl and VOCl monolayers, showing interatomic distances. (c) Side view of structure of heterobilayer FeOCl/VOCl. Dashed lines mark the boundaries of the unit cells used in our DFT calculations.

energies for different configurations is shown in Table I. Our PBE+ $U$  calculations show that the AF and FM spin configurations are the stable phases for FeOCl and VOCl monolayer, respectively, in agreement with previous works<sup>13,42,43</sup>. In both compounds the ground states magnetization is lying along the [010] axis, the spin points along the V-O/Fe-O bond direction, projected along the plane of the layer.

### B. Spin model

Given the insulating nature of the monolayers, we propose a spin model to describe the DFT calculations. The model has 3 types of terms, first-neighbour isotropic Heisenberg exchange, first-neighbour anisotropic exchange (ae) and single ion anisotropy (sia):

$$H = H_{\text{Heis}} + H_{\text{ae}} + H_{\text{sia}}, \quad (1)$$

where:

$$H_{\text{Heis}} = \sum_{i,i'} \frac{J}{2} \vec{S}(i) \cdot \vec{S}(i') \quad (2)$$

$$H_{\text{ae}} = \frac{J_y}{2} \sum_{i,i'} S_y(i) S_y(i') + \frac{J_z}{2} \sum_{i,i'} S_z(i) S_z(i'), \quad (3)$$

, and:

$$H_{\text{sia}} = \sum_i (E(S_x(i)^2 - S_z(i)^2) - DS_y(i)^2). \quad (4)$$

In the sums above  $i$  runs over all the lattice sites of a square lattice and  $i'$  runs over the 4 first neighbours of  $i$ . The first term accounts for first-neighbour isotropic exchange and the third term accounts for single ion anisotropy that reflects the symmetry of the crystal field of Fe and V atoms. In total, we have 5 parameters  $J, E, D, J_y, J_z$ . We estimate them using 6 DFT calculations (see Appendix) and then we test the model with the remaining two. The results of the fitting gives an error with respect the DFT calculations of 7.95 % and 6.09 % for FeOCl and VOCl, respectively, which is rather satisfactory.

In both cases the single ion anisotropies  $D, E$  are larger than the anisotropic exchange constants  $J_y, J_z$ . However, this difference is much smaller in the case of FeOCl. The smaller single ion anisotropy values in this case are probably due to the fact that the  $d$  shell is half full for Fe, so that the orbital momentum is 0, even without crystal field quenching. The predominance of single ion anisotropies, in both cases, is to be expected on account of the smaller atomic weight of the ligands, and thereby smaller spin-orbit coupling. We also note that the proposed model has two main limitations: it only considers first neighbour exchange and it completely ignores magneto-elastic interactions, that are known to be important for VOCl.<sup>14</sup>

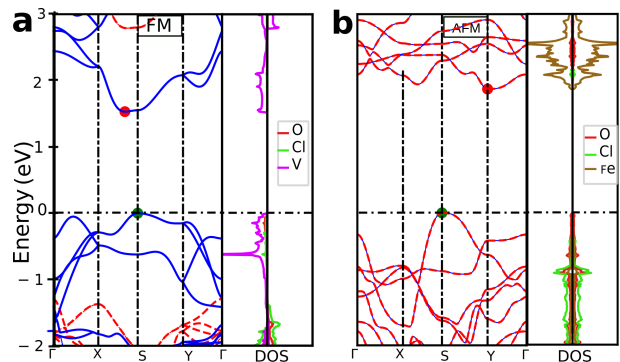


FIG. 2. Band structure of monolayer FeClO-AF and VOCl-FM calculated within PBE+ $U$ . The projected DOS is represented using the atomic color code of Fig. 1.

### IV. ELECTRONIC AND MAGNETIC PROPERTIES HETEROBILAYERS

We now address the electronic and magnetic properties of the VOCl/FeCl heterobilayer. We assume the bulk stacking configuration for the heterobilayer, as shown in Figure 1c. As in the case of monolayers, we have explored several magnetic states. We consistently found that both the magnetic order type and the easy axis of the monolayers is preserved in the heterostructure. This indicates that interlayer exchange is weaker than both the intralayer exchange and the magnetic anisotropy.

The isolated FeOCl has two equivalent Néel states, that are related by time-reversal symmetry (inversion of the magnetization direction). Because of the buckling of the Fe atoms, interlayer exchange breaks this degeneracy, as one of the Fe magnetic sublattices is closer to the vanadium atoms than the other. We refer to these two phases as parallel (p) and anti-parallel (ap), for the FM and AF relative spin orientation of the two closest V-Fe atoms. Our calculations indicate that interlayer exchange is ferromagnetic. The difference of energy difference per unit cell,  $\Delta E_{12}$  between the two states is related to the interatomic exchange as:

$$\Delta E_{12} = j S_V S_{Fe}, \quad (5)$$

where  $j$  is the interlayer exchange coupling. We are ignoring here the small anisotropy of this quantity, which is already small. Indeed, we have  $\Delta E_{12} = 0.14$  meV from which we infer  $j \simeq 0.056$  meV. This interlayer exchange should lead to exchange bias of the hysteresis cycle of the VOCl monolayer as well as the splitting of the otherwise degenerate AF magnons of the FeOCl and very likely their hybridization, at finite  $q$  with the FM magnons of the VOCl bilayer. This hybridization is expected because the AF magnons have a larger  $q = 0$  magnon gap than the FM magnons but a smaller dispersion, on account of their linear dispersion. At the crossing point, interlayer exchange should lead to hybridization gap driven by the

2D Crystal	GS	$E_{[100]}$	$E_{[010]}$	$E_{[001]}$	$E_{[110]}$
FeOCl	FM	54.635	54.396	54.797	54.518
	AF	0.201	<b>0</b>	0.275	0.102
VOCl	FM	0.443	<b>0</b>	1.326	0.236
	AF	24.539	24.071	25.379	24.334
VOCl/FeOCl	AF(Fe)/FM(V)-p	0.585	<b>0</b>	1.614	0.340
	AF(Fe)/FM(V)-ap	0.733	0.140	1.750	0.482

TABLE I. Magnetocrystalline anisotropy energies  $E_{[100]} - E_{[010]}$ ,  $E_{[001]} - E_{[010]}$ , and  $E_{[110]} - E_{[010]}$  (meV/ unit cell). The reference is the total energy of the 101 direction,  $E_{[010]}$ , which in all cases is found to be the ground state. For the heterobilayer AF(Fe)/FM(V)-p stands for parallel spin polarization of neighbor Fe and V atoms and AF(Fe)/FM(V)-ap for anti-parallel spin polarization.

	FeOCl	VOCl
$S$	5/2	1
$J$	2.177 meV	-6.024 meV
$J_y$	-1.6 $\mu$ eV	6.2 $\mu$ eV
$J_z$	3.5 $\mu$ eV	10.7 $\mu$ eV
$D$	5.1 $\mu$ eV	861.1 $\mu$ eV
$E$	-9.5 $\mu$ eV	-430.7 $\mu$ eV
$\epsilon_{110} - \epsilon_{010}$	0.1196 meV	0.2089 meV
$\Delta$ (%)	7.95	6.09

TABLE II. Parameters of the spin model of monolayer FeOCl and VOCl, expressed in meV. The energy difference  $\epsilon_{110} - \epsilon_{010}$  obtained from the model is the AF case for FeOCl and the FM case for VOCl. The error is  $\Delta = |(\Delta_{\text{model}} - \Delta_{\text{DFT}})/(\Delta_{\text{model}} + \Delta_{\text{DFT}})| * 100$ .

interlayer exchange. This will be the subject of future work.

We now discuss the electronic properties of the heterobilayer. Figure 3 shows the band structure and the projected DOS of the most stable magnetic state of the heterobilayer. The bilayer exhibits an indirect bandgap of 1.38 eV. From the projected DOS we determine that the band alignment is type II, similar to the case of heterostructures of transition metal dichalcogenides.<sup>32,44</sup> The top of the VB is mainly composed by V orbitals while the bottom of the CB is dominated by the Fe wave functions. Interestingly, we find that both band extrema feature splittings missing in the monolayer. In the case of the CB, we find a spin-splitting of the Fe bands. This can arise either from the interlayer spin exchange or from the breaking of inversion symmetry of the heterobilayer. The fact that the sign of the splitting is the same for the two interlayer alignments, parallel and antiparallel, discussed above is a strong suggestion that the origin of the splitting is due to the absence of inversion symmetry.<sup>45</sup> On the other hand, the splitting observed in the top of the VB occurs between two states with the same spin and is related to reduced symmetry of the heterobilayer.

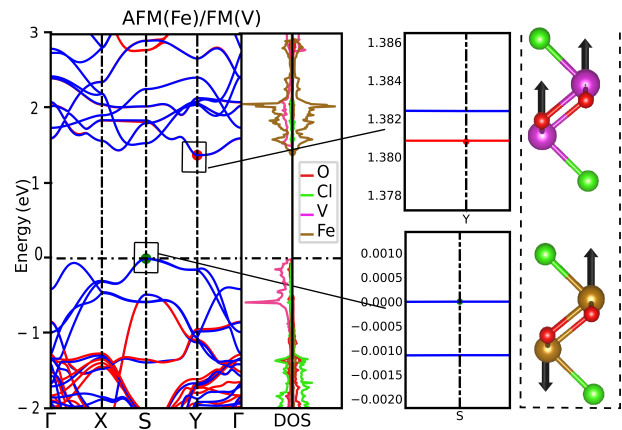


FIG. 3. Band structure of Heterobilayer FeOCl(AFM)/VOCl(FM). Insets show the detail of VBM and CBM and the spin splitting.

## V. CONCLUSIONS

We have characterized the electronic and magnetic properties of VOCl/FeOCl heterobilayers using *ab initio* methods, including the electronic correlation effects within the framework of the Hubbard method. Consistent with experimental work, we find that VOCl (FeOCl) monolayers are ferromagnetic (antiferromagnetic) insulators with an easy axis along the [010] direction. We find a hybrid magnetic order for VOCl/FeOCl heterobilayers, that combines the ferromagnetism of the VOCl monolayer and the antiferromagnetic order in the FeOCl layer. Interlayer exchange is found to be ferromagnetic and should result in a bias of the hysteresis cycle of the VOCl monolayer. Moreover, the reduced symmetry of the heterobilayer causes a spin splitting of both conduction and valence band edges of  $\simeq 2$  meV. The heterobilayer has a type-II band alignment, with the conduction/valence band localized in the Fe(V) layer. Interestingly, combined with the spin splitting of the valence band states, interlayer excitons in this system would have a well-defined spin polarization. Therefore, the magnetic properties can be combined with a long lifetime for the excitons. We also foresee the emergence of hybrid magnon modes combining the AF and FM magnons of both layers.

## VI. ACKNOWLEDGMENTS

This work has been supported by the Algerian Ministry of High Education and Scientific Research under the PNE programme. F. M. thanks the hospitality of the Departamento de Física Aplicada at the Universidad de Alicante and we also thank W. Aggoune for his outstanding help and valuable advice. A. M.-S. acknowledges the Ramón y Cajal programme (grant RYC2018-024024-I; MINECO, Spain) and the Marie-Curie-COFUND pro-

gram Nano TRAIN For Growth II (Grant Agreement 713640). Ab initio simulations were performed on the Tirant III cluster of the Servei d'Informàtica of the University of Valencia. J. F.-R. acknowledges financial support from Generalitat Valenciana funding Prometeo2017/139, FEDER/Junta de Andalucía CTEICU, grant Proyecto PY18-4834 and MINECO-Spain (Grant No.PID2019-109539GB).

### Appendix A: Determination of parameters of the spin model

The parameters  $J$ ,  $J_y, J_z$   $D$  and  $E$  are calculated from the classical energies per atom:

$$\epsilon_\eta(\vec{n}) \equiv \frac{E_{\eta=\pm 1}(\vec{n})}{N_{\text{at}}} = S^2 \frac{\eta z (J + J_y n_y^2 + J_z n_z^2)}{2} + S^2 (E(n_x^2 - n_z^2) - D n_y^2), \quad (\text{A1})$$

where  $\eta = +1(-1)$  stands for FM (AF) configurations,  $S = 1, 5/2$  is the spin offor V and Fe, respectively,  $z = 4$  is the number of first neighbours, and  $\vec{n} = (n_x, n_y, n_z)$  is the unitary vector that marks the different orientations of the magnetic moments. The single ion magnetic anisotropy does not depend on  $\eta$ . We obtain 6 configurations (FM and AF) for the three different orientations of the magnetic moments along the crystal axis:

$$\epsilon_\eta(n_x) \equiv \frac{E_{\eta=\pm 1}(n_x)}{N_{\text{at}}} = S^2 \frac{\eta z (J)}{2} + S^2 (E(n_x^2)),$$

$$\epsilon_\eta(n_y) \equiv \frac{E_{\eta=\pm 1}(n_y)}{N_{\text{at}}} = S^2 \frac{\eta z (J + J_y n_y^2)}{2} + S^2 (-D n_y^2),$$

$$\epsilon_\eta(n_z) \equiv \frac{E_{\eta=\pm 1}(n_z)}{N_{\text{at}}} = S^2 \frac{\eta z (J + J_z n_z^2)}{2} + S^2 E(-n_z^2).$$

In order to derive  $J$  we can use:

$$\epsilon_{FM}(100) - \epsilon_{AF}(100) = S^2 z J. \quad (\text{A2})$$

We now can obtain  $J_y$  and  $J_z$  from

$$\epsilon_{FM}(010) - \epsilon_{AF}(010) = S^2 z J + S^2 z J_y \quad (\text{A3})$$

and

$$\epsilon_{FM}(001) - \epsilon_{AF}(001) = S^2 z J + S^2 z J_z \quad (\text{A4})$$

In order to derive the single ion anisotropies,  $E$  and  $D$  we now compare FM energies along different directions:

$$\epsilon_{FM}(100) - \epsilon_{FM}(010) = D S^2 + E S^2 + \frac{J_y z S^2}{2} \quad (\text{A5})$$

and

$$\epsilon_{FM}(001) - \epsilon_{FM}(010) = D S^2 - E S^2 + \frac{J_y z S^2}{2} - \frac{J_z z S^2}{2} \quad (\text{A6})$$

with two equations and two unknowns. Table II summarizes the parameters of monolayer FeOCl and VOCl obtained from the DFT values of Table I.

- <sup>1</sup> X. Wang, K. Du, Y. Y. F. Liu, P. Hu, J. Zhang, Q. Zhang, M. H. S. Owen, X. Lu, C. K. Gan, P. Sengupta, *et al.*, *2D Materials* **3**, 031009 (2016).
- <sup>2</sup> J.-U. Lee, S. Lee, J. H. Ryoo, S. Kang, T. Y. Kim, P. Kim, C.-H. Park, J.-G. Park, and H. Cheong, *Nano letters* **16**, 7433 (2016).
- <sup>3</sup> B. Huang, G. Clark, E. Navarro-Moratalla, D. R. Klein, R. Cheng, K. L. Seyler, D. Zhong, E. Schmidgall, M. A. McGuire, D. H. Cobden, W. Yao, D. Xiao, P. Jarillo-Herrero, and X. Xu, *Nature* **546**, 270 (2017).
- <sup>4</sup> M. Gibertini, M. Koperski, A. F. Morpurgo, and K. S. Novoselov, *Nature Nanotechnology* **14**, 408 (2019).
- <sup>5</sup> L. Chen, J.-H. Chung, B. Gao, T. Chen, M. B. Stone, A. I. Kolesnikov, Q. Huang, and P. Dai, *Phys. Rev. X* **8**, 041028 (2018).
- <sup>6</sup> A. T. Costa, D. L. R. Santos, N. M. R. Peres, and J. Fernández-Rossier, *2D Materials* **7**, 045031 (2020).
- <sup>7</sup> B. Ding, Z. Li, G. Xu, H. Li, Z. Hou, E. Liu, X. Xi, F. Xu, Y. Yao, and W. Wang, *Nano Letters* **20**, 868 (2019).
- <sup>8</sup> Y. Deng, Y. Yu, M. Z. Shi, Z. Guo, Z. Xu, J. Wang, X. H. Chen, and Y. Zhang, *Science* **367**, 895 (2020).
- <sup>9</sup> L. M. Canonico, T. P. Cysne, A. Molina-Sanchez, R. B.

- Muniz, and T. G. Rappoport, *Phys. Rev. B* **101**, 161409 (2020).
- <sup>10</sup> T. P. Lyons, D. Gillard, A. Molina-Sánchez, A. Misra, F. Withers, P. S. Keatley, A. Kozikov, T. Taniguchi, K. Watanabe, K. S. Novoselov, *et al.*, *Nature Communications* **11**, 6021 (2020).
- <sup>11</sup> S. Kezilebieke, M. N. Huda, V. Vaño, M. Aapro, S. C. Ganguli, O. J. Silveira, S. Głodzik, A. S. Foster, T. Ojanen, and P. Liljeroth, *Nature* **588**, 424 (2020).
- <sup>12</sup> D. R. Klein, D. MacNeill, J. L. Lado, D. Soriano, E. Navarro-Moratalla, K. Watanabe, T. Taniguchi, S. Manni, P. Canfield, J. Fernández-Rossier, and P. Jarillo-Herrero, *Science (New York, N.Y.)* **360**, 1218 (2018).
- <sup>13</sup> S. Glawion, M. R. Scholz, Y. Z. Zhang, R. Valentí, T. Saha-Dasgupta, M. Klemm, J. Hemberger, S. Horn, M. Sing, and R. Claessen, *Physical Review B - Condensed Matter and Materials Physics* **80**, 2 (2009).
- <sup>14</sup> A. C. Komarek, T. Taetz, M. T. Fernández-Díaz, D. M. Trots, A. Möller, and M. Braden, *Physical Review B - Condensed Matter and Materials Physics* **79**, 1 (2009), arXiv:0902.0544.
- <sup>15</sup> M. Ekholm, A. Schönleber, and S. Van Smaalen, *Jour-*

- nal of Physics Condensed Matter **31** (2019), 10.1088/1361-648X/ableff, arXiv:1902.06217.
- 16 S. Yan, P. Wang, C. Y. Wang, T. Xu, Z. Li, T. Cao, M. Chen, C. Pan, B. Cheng, L. Sun, S. J. Liang, and F. Miao, *Science China Information Sciences* **62**, 14 (2019).
  - 17 S. R. Hwang, W. H. Li, K. C. Lee, J. W. Lynn, and C. G. Wu, *Physical Review B - Condensed Matter and Materials Physics* **62**, 14157 (2000).
  - 18 J. P. Bonacum, A. O'Hara, D. L. Bao, O. S. Ovchinnikov, Y. F. Zhang, G. Gordeev, S. Arora, S. Reich, J. C. Idrobo, R. F. Haglund, S. T. Pantelides, and K. I. Bolotin, *Physical Review Materials* **3**, 1 (2019), arXiv:1903.00753.
  - 19 R. W. Grant, *Journal of Applied Physics* **42**, 1619 (1971).
  - 20 A. Schönleber, J. Angelkort, S. van Smaalen, L. Palatinus, A. Senyshyn, and W. Morgenroth, *Physical Review B* **80**, 064426 (2009).
  - 21 M. A. McGuire, G. Clark, K. Santosh, W. M. Chance, G. E. Jellison Jr, V. R. Cooper, X. Xu, and B. C. Sales, *Physical Review Materials* **1**, 014001 (2017).
  - 22 W. Wang, R. Sun, S. He, Z. Jia, C. Su, Y. Li, and Z. Wang, *2D Materials* **8**, 015027 (2021), publisher: IOP Publishing.
  - 23 S. KIM, J. KANG, S. HWANG, and H. KIM, *BULLETIN OF THE KOREAN CHEMICAL SOCIETY* **16**, 299 (1995).
  - 24 W. Zhu, Q. Cui, M. Adam, Z. Liu, L. Zhang, Z. Dai, Y. Yin, S. Chen, and L. Song, *2D Materials* **8**, 025010 (2020).
  - 25 X. J. Yang, X. M. Xu, J. Xu, and Y. F. Han, *Journal of the American Chemical Society* **135**, 16058 (2013).
  - 26 P. Gao, C. Wall, L. Zhang, M. A. Reddy, and M. Fichtner, *Electrochemistry Communications* **60**, 180 (2015).
  - 27 P. Gao, X.-M. Lin, M. A. Reddy, L. Zhang, T. Diemant, R. J. Behm, and M. Fichtner, *Journal of The Electrochemical Society* **163**, A2326 (2016).
  - 28 K. Kim, S. Y. Lim, J. Kim, J.-U. Lee, S. Lee, P. Kim, K. Park, S. Son, C.-H. Park, J.-G. Park, and H. Cheong, *2D Materials* **6**, 041001 (2019).
  - 29 D. Soriano, M. I. Katsnelson, and J. Fernández-Rossier, *Nano Letters* **20**, 6225 (2020), pMID: 32787171, <https://doi.org/10.1021/acs.nanolett.0c02381>.
  - 30 K. Hejazi, Z.-X. Luo, and L. Balents, *Proceedings of the National Academy of Sciences* **117**, 10721 (2020).
  - 31 T. H. Hsieh, H. Ishizuka, L. Balents, and T. L. Hughes, *Phys. Rev. Lett.* **116**, 086802 (2016).
  - 32 E. Torun, H. P. C. Miranda, A. Molina-Sánchez, and L. Wirtz, *Phys. Rev. B* **97**, 245427 (2018).
  - 33 K. Burke and L. O. Wagner, *International Journal of Quantum Chemistry* **113**, 96 (2013), <https://onlinelibrary.wiley.com/doi/pdf/10.1002/qua.24259>.
  - 34 J. P. Perdew, K. Burke, and M. Ernzerhof, *Physical Review Letters* **77**, 3865 (1996), arXiv:0927-0256(96)00008 [10.1016].
  - 35 D. Joubert, *Physical Review B - Condensed Matter and Materials Physics* **59**, 1758 (1999).
  - 36 G. Kresse and J. Furthmüller, *Physical Review B - Condensed Matter and Materials Physics* **54**, 11169 (1996).
  - 37 V. I. Anisimov, J. Zaanen, and O. K. Andersen, *Physical Review B* **44**, 943 (1991).
  - 38 V. I. Anisimov, F. Aryasetiawan, and A. I. Lichtenstein, *Journal of Physics Condensed Matter* **9**, 767 (1997).
  - 39 S. Grimme, J. Antony, S. Ehrlich, and H. Krieg, *Journal of Chemical Physics* **132** (2010), 10.1063/1.3382344.
  - 40 M. D. Lind, *Acta Crystallographica Section B Structural Crystallography and Crystal Chemistry* **26**, 1058 (1970).
  - 41 A. Haase and G. Brauer, *Acta Crystallographica Section B: Structural Crystallography and Crystal Chemistry* **31**, 2521 (1975).
  - 42 S. Wang, J. Wang, and M. Khazaei, *Physical Chemistry Chemical Physics* **22**, 11731 (2020).
  - 43 N. Mounet, M. Gibertini, P. Schwaller, D. Campi, A. Merkys, A. Marrazzo, T. Sohier, I. E. Castelli, A. Cepellotti, G. Pizzi, and N. Marzari, *Nature Nanotechnology* **13**, 246 (2018), arXiv:1611.05234.
  - 44 K. Kośmider and J. Fernández-Rossier, *Physical Review B* **87**, 075451 (2013).
  - 45 D. Soriano and J. Fernández-Rossier, *Physical Review B* **85**, 195433 (2012).